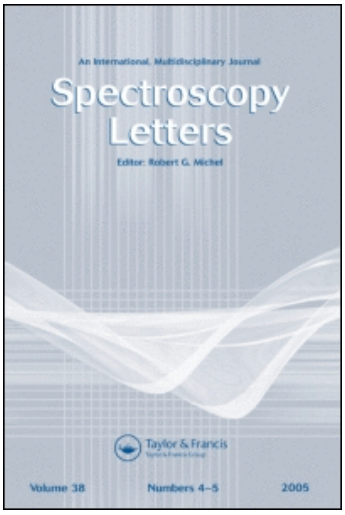

Spectroscopy Letters
Publication details, including instructions for authors and subscription information:
http://www.informaworld.com/smpp/title~content=t713597299

The Reduction of Re^{3+} in Srb_6O_{10} Prepared in Air and the Luminescence of Srb_6O_{10}:Re^{2+}(Re=Eu, Sm, Tm)

Qinghua Zeng[a]; Zhiwu Pei[a]; Shubing Wang[a]; Qiang Su[a]
[a] Laboratory of Rare Earth Chemistry and Physics, Changchun Institute of Applied Chemistry, Chinese Academy of Sciences, Changchun, P. R. China

To cite this Article Zeng, Qinghua , Pei, Zhiwu , Wang, Shubing and Su, Qiang(1999) 'The Reduction of Re^{3+} in Srb_6O_{10} Prepared in Air and the Luminescence of Srb_6O_{10}:Re^{2+}(Re=Eu, Sm, Tm)', Spectroscopy Letters, 32: 6, 895 — 912
To link to this Article: DOI: 10.1080/00387019909350036
URL: http://dx.doi.org/10.1080/00387019909350036

SPECTROSCOPY LETTERS, 32(6), 895–912 (1999)

THE REDUCTION OF RE^{3+} IN SrB_6O_{10} PREPARED IN AIR AND THE LUMINESCENCE OF $SrB_6O_{10}:RE^{2+}$ (RE=Eu, Sm, Tm)

Keywords: luminescence; Strontium borates; rare earth ions; f-d and f-f transitions.

Qinghua Zeng, Zhiwu Pei, Shubing Wang and Qiang Su

Laboratory of Rare Earth Chemistry and Physics, Changchun Institute of Applied Chemistry, Chinese Academy of Sciences, Changchun, 130022, P. R. China

ABSTRACT

The reduction of RE^{3+} to RE^{2+} (RE=Eu, Sm and Tm) in SrB_6O_{10} prepared in air by high-temperature solid state reaction was observed. The luminescent properties of Eu^{2+} and Tm^{2+} show f-d transition and Sm^{2+} shows f-f transition at room temperature. Three crystallographic sites for Sm^{2+} in matrix are available. Vibronic transition of $^5D_0$-$^7F_0$ of Sm^{2+} was studied. The coupled phonon energy about 108 cm^{-1}, was determined from the vibronic transition. Due to the thermal population from $^5D_0$ level, $^5D_1$-^7F_J (J=0, 1, 2) transitions of Sm^{2+} were observed at room temperature. A charge compensation mechanism is proposed as a possible explanation.

INTRODUCTION

Recently it was reported that Eu^{3+} can be reduced to Eu^{2+} in BaB_8O_{13} by solid state reaction at high temperature in air[1]. Literature[2, 3] also reported that the Eu^{3+}, Sm^{3+} and Yb^{3+} could be reduced to the corresponding divalent rare-earth ions in SrB_4O_7 by solid state reaction at high temperature in air. They proposed that the rigid three-dimensional network of BO_4 tetrahedra is necessary to stabilize the divalent rare-earth ions at high temperature in oxidizing atmosphere. Mn^{2+} and Pb^{2+} were reported to retain the divalent state in SrB_6O_{10} by firing in air[4, 5]. It suggests that SrB_6O_{10} should also be a good host to stabilize the divalent rare-earth ions in which also contains the BO_4 tetrahedral network on the basis of its infrared spectrum[6].

The present paper reports on the reduction of RE^{3+} (RE=Eu, Sm and Tm) to RE^{2+} in SrB_6O_{10} and the luminescence of SrB_6O_{10}:RE^{2+}.

EXPERIMENTAL

The preparation of the Eu^{2+}-activated SrB_6O_{10} was carried out according to the literature[6] but heated in air in stead of in H_2/N_2. The dopant Eu ions concentration is 1 mol% of the Sr^{2+} ions in the host compound. The structure of the sample was checked on a Rigaku D/MAX-IIB X-ray powder diffractometer, using Cu $K\alpha_1$ radiation. All samples appear to be single phase and in agreement with JCPDS Card No: 20-1190.

Low-resolution luminescence spectra were performed on a SPEX DM3000f spectrofluorometer equipped with 0.22m SPEX 1680 double monochromators (resolution 0.1 nm) and a 450 W xenon lamp as excitation source. The spectra were not corrected for the lamp output. All the luminescence spectra were recorded at room temperature.

The high-resolution spectra were performed with SPEX-1403 spectrophotometer under the excitation of an N_2 laser beam with flow cryostat

of gaseous helium. The temperature can be varied from 10 K to room temperature.

RESULTS AND DISCUSSION

1. Luminescence of SrB_6O_{10}: Eu^{2+}

The excitation and emission spectra of SrB_6O_{10}: Eu^{2+} prepared in air were shown in Fig.1. There are two broad emission bands peaking at 386 nm and 432 nm, and an excitation spectrum with peak maximum near 305 nm. It is a permitted $4f^65d$-$4f^7$ ($^8S_{7/2}$) transition on the Eu^{2+} ion. Literature[5-7] reported the luminescence properties of Eu^{2+} in this matrix at 4.2K and 77K which was prepared in H_2 stream. They observed three efficient emission band with maxim at 386, 432 and 470 nm with almost the same intensity under 305 nm excitation at 4.2 K. When the temperature increased to 77K, only the emission at 387 and 432 nm were observed and the emission band at 470 nm was quenched. At room temperature, the emission band at 432 nm is quenched to less than 5% of its original intensity. Our results for emission bands with maxima at 386 and 432 nm under 305 nm excitation of SrB_6O_{10}:Eu^{2+} prepared in air is in good agreement with theirs. The spectra suggested that the Eu^{2+} situated more than one lattice site in matrix. This can be confirmed by the high-resolution spectra of Sm^{2+} in SrB_6O_{10} at 10 K.

For divalent europium a high emission intensity and a narrow band width require weak Stokes shift. Due to the high strength of the boron-oxygen bonds, the borates with high B_2O_3 content can form a rigid three-dimensional network which reduces the atomic displacements responsible for the Stokes shift. Among the Eu-doped alkaline earth borates, only the

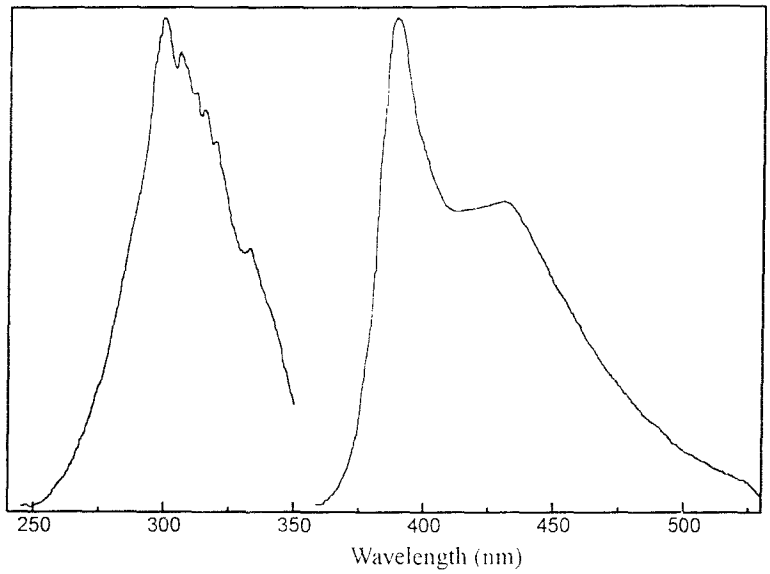

FIG. 1. The excitation and emission spectra of Tm^{2+} in SrB_6O_{10} at room temperature.

B_2O_3-richest phases (SrB_4O_7, SrB_6O_{10}) show weak thermal quenching at 300K[8]. The intensity of Eu^{2+} emission depends strongly on the fraction of the tetrahedral coordination boron atoms in the Sr-borates. In these borates, the Eu^{2+}-doped SrB_4O_7 has the highest quantum efficiency and shows the strongest emission intensity while the other Sr-borates show weaker luminescence.

2.1. The Low-resolution Luminescence of Sm^{2+} in SrB_6O_{10}

The low-resolution emission spectra at room temperature of Sm^{2+} in SrB_6O_{10} prepared in H_2/N_2 and air are shown in Fig.2. It shows that emission spectrum of Sm^{2+} in SrB_6O_{10} prepared in air is identical to those prepared in H_2/N_2 except that a group of weak lines at 562, 600 and 647 nm corresponding to $^4G_{5/2} \rightarrow {}^6H_J$ (J=5/2, 7/2, 9/2 respectively) transitions of Sm^{3+}

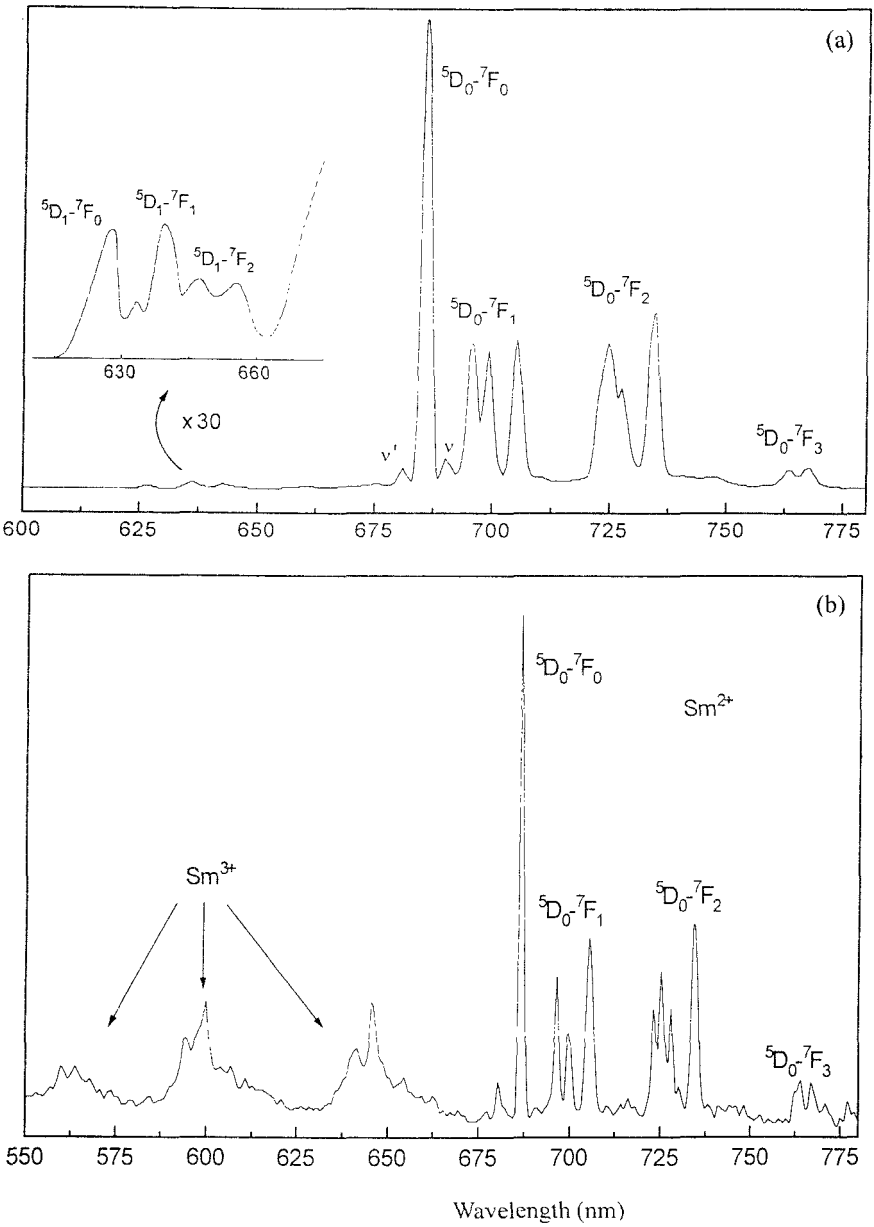

FIG. 2. The low-resolution spectra at room temperature of Sm^{2+} in SrB_6O_{10} prepared in (a) H_2/N_2 (upper) and (b) air (lower). (The inset shows the enlargement of the emission in the range of 620--680 nm).

ions when sample was prepared in air. It is therefore deduced that the Sm^{3+} can be reduced to the divalent state in SrB_6O_{10} prepared at high temperature in air. The emission spectrum contains four groups lines at 685, 700, 725 and 760 nm corresponding to the transitions of $^5D_0$--^7F_J (J=0, 1, 2, 3) transitions of Sm^{2+}, respectively. The dominant line is at 685 nm due to the $^5D_0$--$^7F_0$ transition which shows that Sm^{2+} occupied a crystallographic site without center symmetry.

2.2. The High-resolution Luminescence of Sm^{2+}.

The high-resolution spectra at different temperature was recorded since the temperature dependence of the relative intensities of the lines belonging to the same group is of great help to classify the lines according to the emitting Stark level. The intensity of the lines within each group is roughly evaluated from their heights. Fig. 3 shows the high-resolution emission spectra at 10 K.

It is observed that the transitions of Sm^{2+} in SrB_6O_{10} are from $^5D_0$-^7F_J (J=0, 1, 2, 3). The numbers of the transition lines for $^5D_0$-$^7F_0$ transition are three (designated as Center I, Center II and Center III), for $^5D_0$-$^7F_1$ transition are nine and for $^5D_0$-$^7F_2$ are twelve. Since if the degeneracy of $^7F_1$ energy level for one site is completely lifted and the lines are well-separated, the number of its lines are at most 3, therefore, there are at least three crystal sites for Sm^{2+} in the matrix. The luminescent intensity of Sm^{2+} in Center III is much weaker than those in the other two centers.

Fig.4 shows the high-resolution spectra at 200 and 300 K of Sm^{2+} in the matrix. The differences between them are, firstly, the intensity ratio of Center II to Center I increased with the increasing of temperature while Center III decreased and vanished at 300 K; secondly, in the $^5D_0$--$^7F_1$ transition, three lines at 14456, 14439 and 14422 cm^{-1} disappeared at room

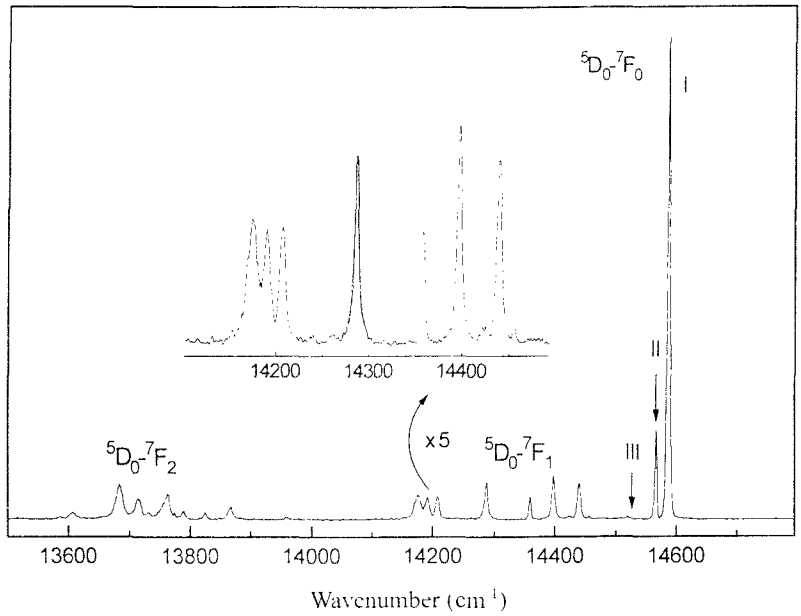

FIG. 3. The high-resolution emission spectra of Sm^{2+} in SrB_6O_{10} at 10 K. (The inset shows the enlargement of $^5D_0$-$^7F_1$ transitions).

temperature. Therefore, these three lines can be assigned to Center III. With the increasing of temperature, Center III was quenched by temperature and Center I and II increased. This implies that the energy transfer from Center III to Center I and II is possible. Such energy transfer process was also observed in the divalent europium in this matrix[5-7] in which energy transfer of Eu^{2+} occurred from Center III to Center II and Center I. It can also be confirmed by the lifetime of these centers as discussed in the following text.

2.3. The Multiphonon Transition of Sm^{2+}.

From Fig. 2, it can be found that there are two weak lines beside two sides of the $^5D_0$--$^7F_0$ transition (14586 cm^{-1}). They are at 680.3 nm (14699

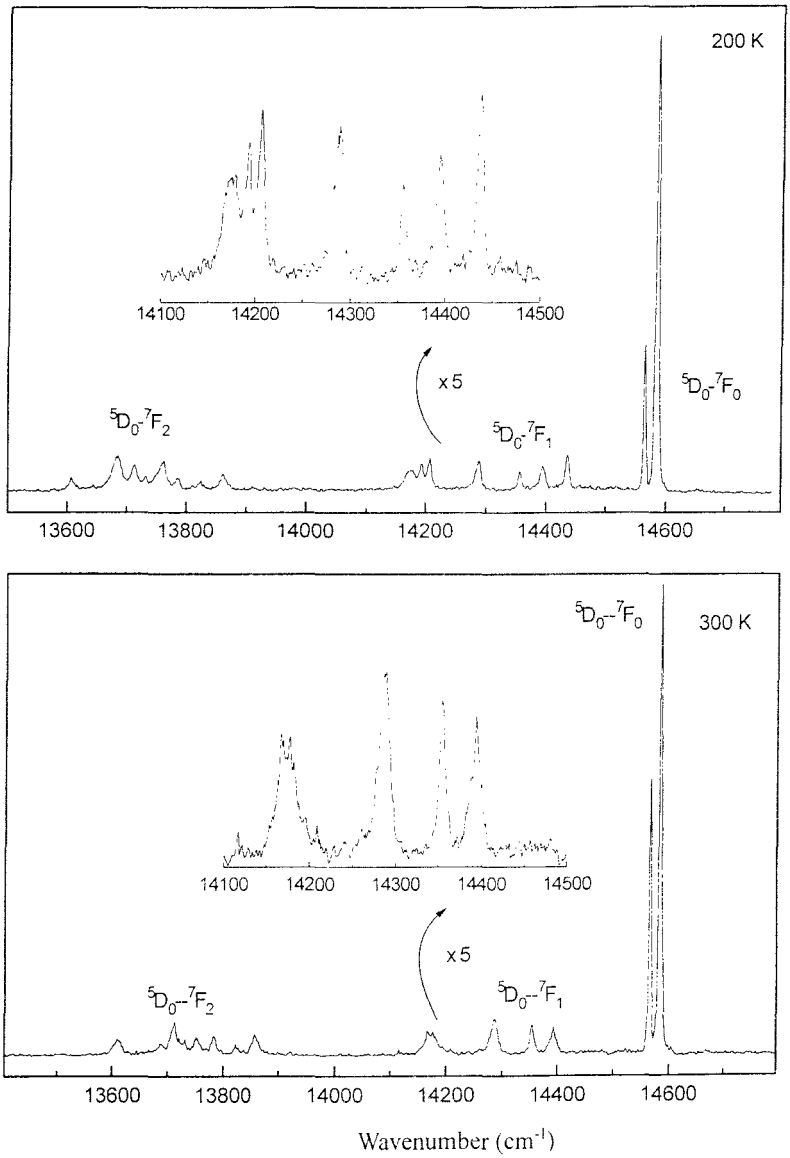

FIG. 4. The high-resolution emission spectra of Sm^{2+} in SrB_6O_{10} at different temperature. (The inset shows the enlargement of $^5D_0$--$^7F_1$ transitions.)

cm^{-1}, denoted as ν') and 690.4 nm (14484 cm^{-1}, donated as ν). Since these lines are too weak and broad and there are only three sites for Sm^{2+}, these weak lines can not be the transitions of Sm^{2+} but the vibronic transitions of the coupling of the 4f electrons with lattice, namely, phonon satellite lines. The $^5D_0$--$^7F_0$ transition at 14586 cm^{-1} is the zero-phonon line (ZPL). The energy difference between Line ν' and ZPL is $\Delta E_{\nu'} \approx 113$ cm^{-1} and the energy difference between Line ν and ZPL is about $\Delta E_{\nu} \approx 104$ cm^{-1}. Therefore, during the transitions, the ZPL has been coupled by phonons with average energy $\hbar\omega \approx (113+104)/2 \approx 108$ cm^{-1}. These phonon lines can be explained by single--configuration--coordinate mechanism in which only those vibration modes with single frequency can couple with the 4f electrons and results in sharp lines. They are originated from the transition in which the $^5D_0$ and $^7F_0$ states have different lattice vibration levels. It can also be found that the intensity of vibronic line ν increases with the increase of temperature. Lines ν and Line ν' can be attributed to the transitions $|^5D_0,n\rangle \rightarrow |^7F_0, n+1\rangle$ and $|^5D_0,n+1\rangle \rightarrow |^7F_0, n\rangle$ respectively, where n is the quantum number of vibration levels of the crystal lattice. Line ν and Line ν' corresponded to P =1 for emitting P phonons and P =-1 for absorbing P phonons, respectively. The intensity ratio of ν and ν' to $^5D_0$ -$^7F_0$ zero-phonon line can be written as[9-11]:

$$I_{\nu} / I_0 = S < 1 + m > = \frac{S}{1 - \exp(\frac{-\hbar\omega}{kT})} \qquad P=1 \qquad (1a)$$

$$I_{\nu'} / I_0 = S < m > = \frac{S \exp(\frac{-\hbar\omega}{kT})}{1 - \exp(\frac{-\hbar\omega}{kT})} \qquad P=-1 \qquad (1b)$$

where k is the Boltzmann constant; S is the Huang-Rhys factor which shows

the coupling strength during the transitions; <m> is Plank's thermal average quantum index: $\langle m\rangle=[\exp(-\hbar\omega/kT)/[1-\exp(-\hbar\omega/kT)]$; T is absolute temperature; $\hbar\omega$ is phonon energy which was coupled during the transition.

From Fig.2, $\hbar\omega\approx108$ cm^{-1}, T=300 K, it can be obtained that the ratio of I_v/I_0 is about 0.013, and Huang-Rhys factor S can be calculated from Eq.(1b) to be S≈0.015; then we obtained the ratio of I_v/I_0 from Eq.(1a) of $I_v/I_0\approx0.037$. This value is close to the experimental result of I_v/I_0 about 0.033.

The total radiative decay rate can be obtained from the spectra. As the decay time is determined by the radiative and non-radiative decay rates. For the $^5D_0$ level, the non-radiative decay rate can be neglected because the energy gap to the next lower level ($^7F_6$) is large (about 10000 cm^{-1}). The highest frequency phonons have an energy of 1400 cm^{-1} in SrB_6O_{10}, so multiphonon relaxation requires 7~8 phonons from $^5D_0$ to $^7F_6$. It is known that the multiphonon relaxation is inefficient for more than seven--phonon processes.

The non-radiative transition rate (A_{NR}) from $^5D_1$ to $^5D_0$ can be calculated by the following equation[9-11]:

$$A_{NR}=N\frac{(S<m+1>)^{P_0}\exp(-S<2m+1>)}{P_0!}$$

$$=N\frac{S^{P_0}<m+1>^{P_0}\exp(-S<2m+1>)}{P_0!} \qquad (2)$$

Here N is the rate constant of non-radiative transition with the order of 10^{11}~10^{14}; $P_0=(\Delta E_{10}/\hbar\omega)$, is the number of the phonons bridging the energy gap between the level of $^5D_1$ and $^5D_0$,. In a given matrix, since the position of $^5D_1$ and $^5D_0$ in Sm^{2+}-doped matrix does not change greatly, the energy gap between these two energy levels is about $\Delta E\approx1350$ cm^{-1}, P_0 depends on the variation of $\hbar\omega$--the lattice-phonon energy in different lattice, so the non-

radiative transition probability, which is the function of P_0 as shown in Eq.(2) will change in different lattice. The phonons with the highest frequency in the lattice will play the main role in the non-radiative transition. Take $N \approx 10^{11} \sim 10^{14}$, $P_0 = 1$, then we found $A_{NR} \approx 4 \times 10^9 \sim 4 \times 10^{13}$. For the comparison of the dependence of $^5D_1 \rightarrow {}^5D_0$ non-radiative transition on the different lattice, let us take another matrix $BaCl_2$ as an example. In $BaCl_2:Sm^{2+}$, $\hbar\omega \approx 200\ cm^{-1}$, $P_0 = \Delta E_{1\sim0}/\hbar\omega \approx 6 \sim 7$. In SrB_6O_{10}, $\hbar\omega \approx 1200\ cm^{-1}$, $P_0 = 1 \sim 2$. Then we can obtain the non-radiative transition probability from $^5D_1$ to $^5D_0$ in SrB_6O_{10} is about $10^7 \sim 10^{15}$ times bigger than in $BaCl_2$. Therefore, no $^5D_1$-^7F_J transitions of Sm^{2+} in SrB_6O_{10} were found even at 10 K while the transition of $^5D_1$-^7F_J can still be observed even at 77 K for Sm^{2+} in $BaCl_2$. However, an interesting phenomenon was found that some weak sharp lines in the range of 620 to 670 nm were observed at room temperature (see Fig.2). These lines must correspond to the $^5D_1$-^7F_J (0, 1, 2) transitions of Sm^{2+} in SrB_6O_{10}. It is due to the fact that the $^5D_1$ level is thermally populated by $^5D_0$ level and results in the transition of $^5D_0 \rightarrow {}^5D_1 \rightarrow {}^7F_J$.

2.4. The Lifetime of $^5D_0$--$^7F_0$ Transition of Sm^{2+} in SrB_6O_{10}.

The lifetime measurements yield information about the kinetics of the luminescence process, such as the fluorescence efficiency, energy transfer, the excitation and de-excitation process.

The lifetime of Sm^{2+} $^5D_0$--$^7F_0$ transition were recorded at different temperatures. The decay curves were presented in Fig. 5 for the lifetime at 300 K. All of the decay curves are in single exponential.

The lifetime for Center I and II at 10 K is about 5.0 ms and 4.5 ms, respectively. At 300 K, the lifetime for these two centers is 4.24 and 2.69

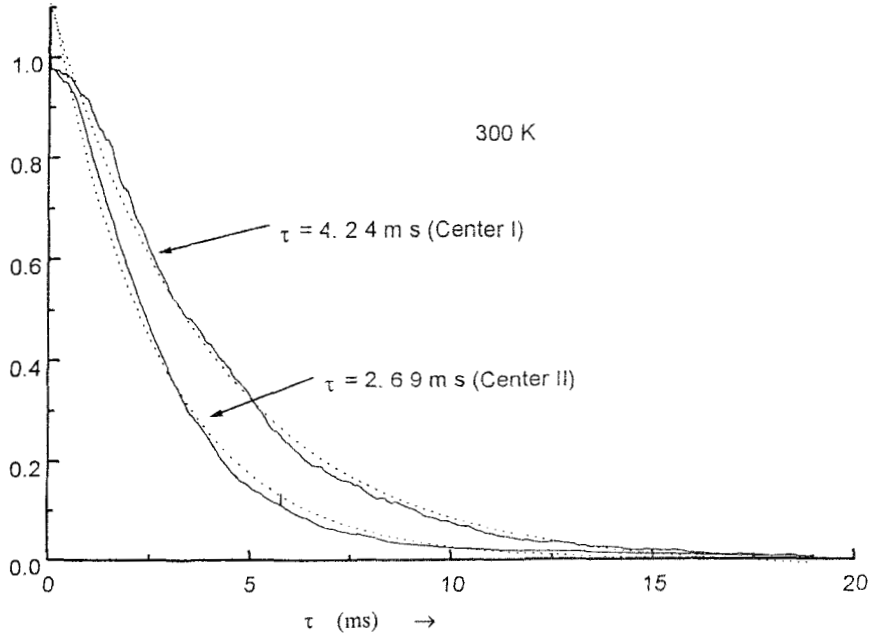

FIG. 5. The lifetime of Center I and II of Sm^{2+} in SrB_6O_{10} at 300 K. (····· experimental; ----- fitted by single exponential decay function: $f(t)=Aexp(-x/\tau)+B$; A, B is constant, respectively).

ms. Due to their different lifetime, it is deduced that the two emission lines at 14586 and 14566 cm^{-1} originate from different luminescent centers.

The dependence of the lifetime of Center I of Sm^{2+} in SrB_6O_{10} as a function of temperature were also performed in the range of 10 K to 300 K. The results were shown in Fig. 6. It shows that the lifetime of Sm^{2+} in Center I is temperature-dependent. The lifetime generally decreases with the increasing of temperature. The lifetime presents a small rise at low temperature, which was possibly due to the energy transfer from Center III to Center II and Center I. With the increasing of temperature, the thermal depopulation, and temperature quenching of $^5D_0$ level became more dominant and resulted in shorter decay time.

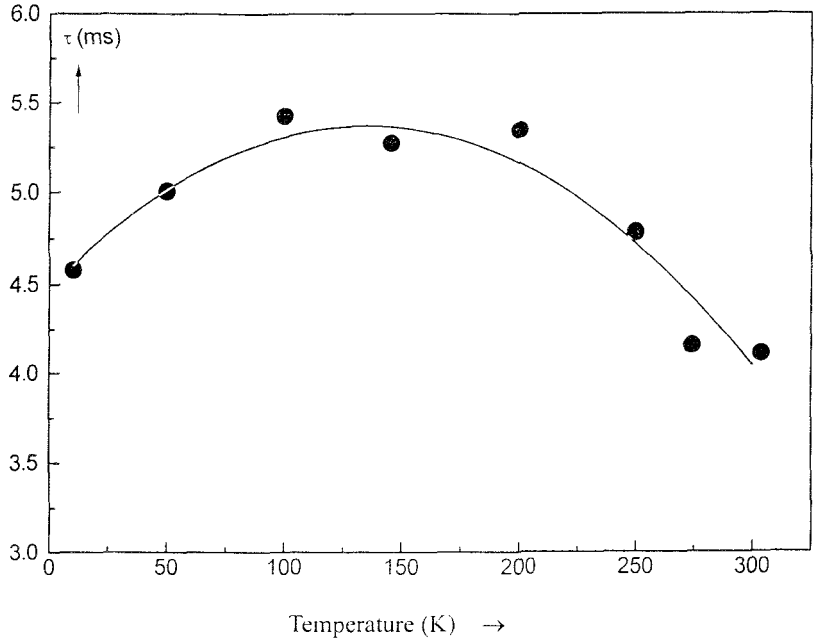

FIG. 6. The dependence of the lifetime of $^5D_0$-$^7F_0$ transition of Sm^{2+} in Center I (14586 cm^{-1}) in SrB_6O_{10} as a function of temperature.

3. The Luminescence of Tm^{2+} in SrB_6O_{10}.

For Tm^{2+}, the splitting of the $4f^{12}(^3H_6)5d(e_g)$ states is almost entirely due to the 4f--5d electrostatic interaction[12]. The excitation and emission spectra at room temperature of Tm^{2+} in SrB_6O_{10} prepared in air were shown in Fig.7. The shape of the spectra is close to that of Tm^{2+} in SrB_4O_7 [2].

The excitation spectrum shows a number of bands in the region of 200 to 500 nm. These bands correspond to the $4f^{13}$--$4f^{12}5d$ transitions. Some narrow and well-separated bands can be seen due to the splitting of the $4f^{12}$ configuration in $4f^{12}5d$ level by the crystal-field with the splitting energy at about ΔE=5480 cm^{-1}. The maximum excitation band is at about 380 nm.

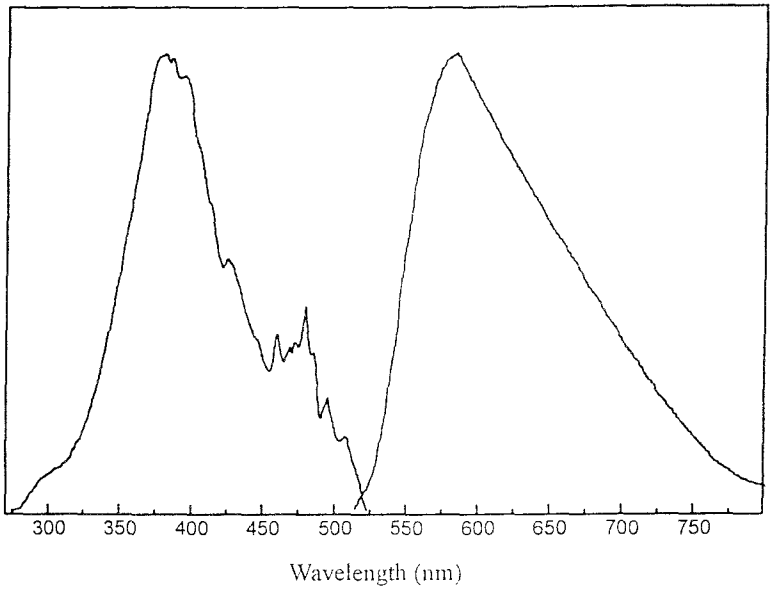

FIG. 7. The excitation and emission spectra of Tm^{2+} in SrB_6O_{10} at room temperature.

The lowest excitation band is at 480 nm which was in a higher energy side than in CaF_2.[13] In CaF_2, the lowest energy is at 600 nm due to the transitions to the $4f^{12}$ $(^3H_6)5d(e_g)$states. This is due to the high degree of ionicity in the lattice and a small crystal-field splitting of the $4f^{12}5d$ state. The excitation band of SrB_6O_{10}:Tm^{2+} is similar in form to that of Tm^{2+} in CaF_2 and SrB_4O_7.[13, 14]

The Tm^{2+} in SrB_6O_{10} shows an emission at around 580 nm under the excitation of 480 nm. This emission corresponds to the $4f^{12}5d$--$4f^{13}$ transition. The $4f^{13}$ configuration can also be split by the crystal field into two levels: $^2F_{5/2}$ and $^2F_{7/2}$. Since Tm^{2+} is isoelectronic with Yb^{3+} ion, there will be two $4f^{12}5d$--$4f^{13}$ emission bands: one is a broad band for $4f^{12}5d$--$4f^{13}$ $(^2F_{7/2})$ transition in the visible region, and the other is an emission line for

$4f^{13}(^2F_{5/2})$--$4f^{13}(^2F_{7/2})$ transition in the infrared region. Therefore, the emission band at 580 nm were assigned to the $4f^{12}5d$--$4f^{13}$ $(2F_{7/2})$ transition.

4. Charge Compensation Mechanism

Literature[15] reported that the number of triangularly coordinated boron atoms per tetrahedrally coordinated boron is equal to n-1 for the region greater than n=1when the borates are written in the form $M_xO{\bullet}nB_2O_3$. For $SrB_6O_{10}(SrO{\bullet}3B_2O_3)$, n-1=2, therefore, it contains four triangularly and two tetrahedrally coordinated boron atoms. Literature[6] reported that SrB_6O_{10} consists of a three-dimensional network of B_3O_5 rings containing two triangular and one tetrahedral boron atoms on the basis of its infrared spectrum pattern. However, the structure of SrB_6O_{10} is still unelucidated by far.

When the trivalent RE^{3+} ion occupies the lattice site of divalent Sr^{2+}, two RE^{2+} ions should be needed to substitute three Sr^{2+} ions in order to keep the charge balance. Hence a vacancy defect at the Sr^{2+} site formed. This vacancy defect is represented as V_{Sr}'' with two negative charges due to the absence of Sr^{2+} and then it becomes a donor of electrons while the two RE^{3+} ions become acceptors of electrons. Consequently, the negative charges in the charged vacancy defects will be transferred into the RE^{3+} ion site and the trivalent Eu^{3+} ion was reduced to the divalent state RE^{2+}. Here, if this vacancy defect can be regarded as an associate, the association should be represented by the Kroger and Vink's notation[16]:

$$V_{Sr}''+2RE_{Sr}^{\bullet}=[(RE_{Sr})_2V_{Sr}]^{\times}$$

Literature[17] reported that Eu^{3+} can be reduced to the divalent state ions in the high-pressure phase of SrB_2O_4(III) and SrB_2O_4(IV) in H_2 but no Eu^{2+} existed in Eu^{3+}--doped $Sr_2B_2O_5$ and SrB_2O_4 (I) (atmosphere pressure phase) even prepared in hydrogen flow, and only a very small amount of Eu^{2+} in

$Sr_3B_2O_6$ with considerable effort. Such results can be explained that since $Sr_3B_2O_6$, $Sr_2B_2O_5$ and SrB_2O_4 (I) contain only planar triangular BO_3 units, the charge compensation would take place by introducing one interstitial oxygen ion per two Eu^{3+} ions rather than by forming a negatively charged vacancy defect. The interstitial oxygen ion links two planar BO_3 groups and form two corner sharing BO_4 tetrahedra[7], hence the Eu^{3+} ion still retains its trivalent state in these matrices. In the high pressure phase of SrB_2O_4 (III) and SrB_2O_4(IV), the hosts contain BO_4 tetrahedral units which can prevent the Eu^{2+} from being attacked by the oxygen.

As discussed above, it can be seen that the reduction of Eu^{3+} depends strongly on the structure of the boron units. The three-dimensional network of BO_4 tetrahedra plays a role of shield, it can isolate the Eu^{2+} ions from each other and completely or partly surround the Eu^{2+} ions and resist the attack of the oxygen, so Eu^{2+} ions can retain the divalent state in air even at high temperature. This can be verified from the different oxidation temperature for europium borates: 673K for $Eu_3B_2O_6$, 683K for $Eu_2B_2O_5$, 753K for EuB_2O_4 and 1033K for EuB_4O_7. $Eu_3B_2O_6$ and $Eu_2B_2O_5$ contain BO_3^{3-} and $B_2O_5^{4-}$ ion respectively, and EuB_2O_4 consists of $(BO_2)_\infty$ chains. The Eu^{2+} ions in SrB_4O_7 located in the 'cage' of BO_4 units, completely surrounded by these units of $(B_4O_7)_\infty$ network, and therefore it becomes too difficult to be attacked by oxygen[18]. However, no information has been found to discuss the structure of REB_6O_{10} ; until now it was thought that all Eu(II)-borates are isostructural with the corresponding Sr-borates because of their closely similar effective ionic radii.

CONCLUSIONS

The RE^{3+} (RE=Eu, Sm and Tm) ions can be reduced to the corresponding RE^{2+} ions in SrB_6O_{10} in air by high-temperature solid-state

reaction. The investigation on valence change and luminescence of RE^{2+} (RE=Eu, Sm and Tm) ions in SrB_6O_{10} prepared in air shows that the matrix SrB_6O_{10} is a good host for the divalent rare earth ions. The rigid framework of BO_4 tetrahedral units in the structure of the matrix plays a significant role in stabilizing the divalent rare-earth ions in air at high temperature. Three crystallographic cation sites are available for Sr^{2+} (Sm^{2+}) in the host lattice using Sm^{2+} as the structure probe. From 10 to 300 K, with the increasing of temperature, there is energy migration within Sm^{2+} ions from Center III to Center II and Center I. At 300 K, the emission of Sm^{2+} in Center III is completely quenched by temperature. $^5D_1$--^7F_J transitions appeared at room temperature due to the thermal population inversion. The phonon lines are found at room temperature beside the zero-phonon line of Sm^{2+} with energy about 108 cm^{-1} due to the coupling of the excited 4f electrons with local phonons. The luminescence of divalent thulium shows that the $4f^{12}5d$ band in the lattice is situated at a relatively higher energy position. The emission takes place in $4f^{13}$--$4f^{12}5d$ configuration in the visible region with a maximum at about 580 nm.

ACKNOWLEDGMENT

This work was supported by National Key Project for Fundamental Research and the National Natural Science Foundation of China.

REFERENCES

1. Zeng Q., Pei Z., Wang S., Su Q., Mater. Res. Bull., (to be published).

2. Peterson J., Xu W., Dai S., Chem. Mater. 1995; 7: 1686

3. Pei Z., Su Q., Zhang J., J. Alloys and Compds., 1993; 198: 51.

4. Koskentalo T., Leskela M., Niinisto L., Mater. Res. Bull., 1985; 20: 265.

5. Leskla M., Koskentalo T., Blasse G., J. Solid State Chem., 1985; 59: 272.

6. Machida K., Adachi G., Shiokawa J., J. Luminesc., 1979; 21: 101.

7. Schipper W., Voort D., Berg P., Vroon Z., Blasse G., Mater. Chem. Phys., 1993; 33: 311.

8. Fu W., Fouassier C., Hagenmuller P., Mater. Res. Bull., 1987; 22: 899.

9. Huang K., Rhys A., Proc. Roy. Soc. (London), 1950, A204:406

10. Peker S., Zh. Eksp. Teor. Fiz. 1950, 20: 510.

11. Struck C. W. Fonger W., J. Chem. Phys. 1974, 60: 1988.

12. Sugar J. Opt. Soc. Am. 1970; 60: 454.

13. Kiss Z., Phys. Rev. 1962; 127: 718.

14. Schipper W., Meijerink A., Blasse G., J. Lumin. 1994; 62: 55.

15. Block S., Piermarim G., Phys. Chem. of Glasses., 1964; 5(5): 138.

16. Kroger F., The Chemistry of Imperfect Crystals (North-Holland, Amsterdam, 1964)

17. Machida K., Adachi G., Shiokawa J., Shimada M. and Koizumi M., Inorg. Chem., 1980; 19: 983 .

18. Machida K., Adachi G., Shiokawa J., Acta Crystallogr., 1980; B36: 2008.

Date Received: August 24, 1998
Date Accepted: July 10, 1999